Eur Biophys J (2003) 32: 355–362
DOI 10.1007/s00249-003-0285-z

ARTICLE

Xiangqun Xu · Ruikang K Wang · Alicia El Haj

Investigation of changes in optical attenuation of bone and neuronal cells in organ culture or three-dimensional constructs in vitro with optical coherence tomography: relevance to cytochrome oxidase monitoring

Received: 4 April 2002 / Revised: 18 November 2002 / Accepted: 20 January 2003 / Published online: 12 March 2003

Abstract Changes in optical attenuation, relevant to cytochrome oxidase, of the rat bone periosteal tissue in explanted culture and human neuronal cells in three-dimensional agarose constructs have been monitored by the use of optical coherence tomography (OCT), with potential applications in tissue engineering and diagnosis. A superluminescent diode (SLD) with a peak emission wavelength ($\lambda = 820$ nm) that is the near-infrared absorption band of the oxidized form of CytOx was employed. The attenuation coefficient was obtained from the depth-resolved reflectance profiles of liquid phantoms (naphthol green B with intralipid), explant culture (periosteum of calvaria from rats) and cells in 3D agarose constructs. The absorption coefficient of naphthol green B can be accurately quantified by the linear relationship between attenuation coefficients and the concentration. The difference in the attenuation coefficient of astrocytoma cells in agarose before and after reduction of CytOx is 0.26 ± 0.10 mm^{-1} ($n = 9$), whereas no attenuation is observed with the agarose control. Reduction of the enzyme in periosteal tissue leads to a change in attenuation coefficient of 0.43 ± 0.24 mm^{-1} ($n = 7$). For comparison, using a biochemical assay, the absorption coefficient of the oxidized-reduced form of CytOx is measured at approximately $8.3 \pm 1.5 \times 10^{-3}$ mm^{-1} ($n = 4$) and $8.7 \pm 2.5 \times 10^{-3}$ mm^{-1} ($n = 4$) at 820 nm for astrocytoma cells and rat periosteum, respectively. The lower value of CytOx concentration using biochemical versus OCT measurements may result from shifts in the scattering profile and the amplifying influences of multiple heme-based oxidases, indicating that conventional OCT is not specific enough to monitor redox changes in cytochrome oxidase. However, qualitative shifts in oxidation state are apparent using the technique. Our results suggest the potential application of OCT in providing high-resolution tomographic imaging of tissues in organ culture and cells grown in three-dimensional constructs in vitro.

Keywords Absorption · Cytochrome oxidase · Optical coherence tomography · Scattering · Tissue and cells

X. Xu · R.K. Wang (✉) · A. El Haj
Centre for Science & Technology in Medicine,
School of Medicine,
Keele University/North Staffordshire Hospital Trust,
Stoke-on-Trent, ST4 7QB, UK
E-mail: r.k.wang@cranfield.ac.uk
Tel.: +44-1525-863450
Fax: +44-1525-863533

Present address: R.K. Wang
Institute of KBioscience and Technology,
Cranfield University, Silsoe,
Bedfordshire, MK45 4DT, UK

Introduction

Optical coherence tomography (OCT) is an optical imaging technique that has high axial resolution and high dynamic range by the use of a broadband light source and heterodyne detection technique. It has been shown to be suitable for non-invasive two-dimensional tomographic imaging of microstructures beneath the tissue surface (Tearney et al. 1997; Wang and Elder 2002a). In addition, OCT provides for one-, two- and three-dimensional images of internal microstructural optical properties such as refractive index, absorption coefficient, scattering coefficient and birefringence. Recently, this technique has been used to determine analyte concentrations in scattering media (Sathyam et al. 1999), to measure optical properties of tissues (Schmitt et al. 1993a), to derive spectroscopic information from tissue phantoms (Schmitt et al. 1998) and tissues (Morgner et al. 2000) and to investigate the optical clearing of soft tissue (Wang et al. 2001; Wang and Elder 2002b) and whole blood (Tuchin et al. 2002).

Mitochondria cytochrome *c* oxidase (CytOx) is a terminal enzyme in the respiratory chain. The reaction that this enzyme catalyzes is linked to the generation of ATP in cells. In the presence of oxygen and absence of substrate, the enzyme is fully oxidized. Changes in CytOx redox state could be useful markers for the

oxygenation state of the tissue owing to its redox changes in response to oxygen availability at the cellular level. Monitoring the redox state of CytOx could thus provide an insight into cellular activity and viability of tissues.

CytOx has a broad absorption band that is found in the near-infrared region. This band absorbs with a maximum at 830 nm in oxidized CytOx and is bleached on reduction (Tzagoloff 1982). The technique of near-infrared spectroscopy (NIRS) shows great promise for minimally invasive assessment, based on the fact that the NIR absorption signal, which changes with oxygenation, arises from only haemoglobin and CytOx in tissues. NIRS has been studied for monitoring regional blood volume change and extracellular (Hb oxygenation) and intracellular tissue oxygenation (CytOx redox state) (Jöbsis 1977; Delpy and Cope 1997). However, conventional NIRS with a large-area pickup optode is not capable of discriminating the redox change of CytOx as a function of depth in the tissue; moreover, its spatial resolution is severely limited.

In this paper we investigate the possibility of OCT in monitoring the changes in optical property with the redox shift of CytOx in cells and bone tissue. High-resolution images of periosteum overlying calvaria of different age rats were obtained by the OCT system and the decrease in attenuation with redox shift of CytOx in cultured cells and bone tissue was observed. In addition, in this study we attempt to correlate our findings with OCT to CytOx concentration measured using a biochemical assay of the absorption coefficient at 820 nm.

Materials and methods

Theory and system

Figure 1 shows a schematic diagram of the OCT system, based on a fibre optic implementation of a Michelson-type interferometer (for further details, see Wang 1999; Wang et al. 2001). In this system, incident light from a broadband light source is coupled into a fibre, and is split by an optic-fibre coupler. Half of the light is directed towards a moving mirror. This path is known as the reference arm of the interferometer. The remaining light is guided towards the sample with focusing optics. When light reflected from the reference arm is recombined with light that has returned from the sample arm to detector, these two beams interfere only if the optical path lengths of the two beams are matched to within the coherence length of the light. The coherence length of the light source is analogous to the pulse duration for the measurement of the echo delay time. It thus determines the axial resolution of the OCT system. Therefore, a higher axial resolution can be achieved with the choice of a shorter coherence length, i.e. broader spectrum bandwidth of the light source.

The amplitude of the reflected light as a function of depth within the tissue is obtained by scanning the reference mirror with a constant velocity (Fig. 1) and the magnitude of the interferometric fringes is digitized. The result is the measurement of optical backscattering or reflectance, $R(z)$, versus axial ranging distance, or depth, z. The reflectance depends on the optical properties of tissue, i.e. the absorption (μ_a) and scattering (μ_s) coefficients, or total attenuation coefficient (μ_t), $\mu_t = \mu_a + \mu_s$. The relationship between $R(z)$ and μ_t is, however, very complicated owing to the high scattering nature of biological tissue. However, for relatively

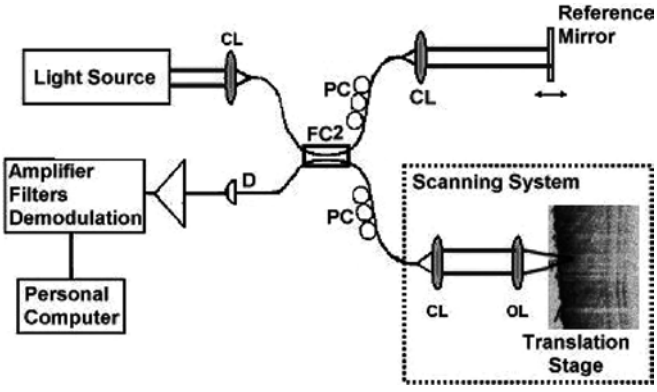

Fig. 1 Schematic diagram of the OCT system used in the experiments, where a light source with central wavelength at 820 nm and bandwidth of 25 nm was employed, delivering an output of 1 mW. *CL* represents the collimating lens, *FC* the fibre optic coupler, *PC* the polarization controller, *OL* the objective lens and *D* the detector

transparent tissue the reflected power will be negatively proportional to $2\mu_t z$ in exponential scale according to the single scattering model that is valid for an optical depth less than 4 (Schmitt et al. 1993b):

$$R(z) = I_0 * T(z) * \exp(-2\mu_t z) \tag{1}$$

where I_0 is the optical power launched into the tissue sample and $T(z)$ is the reflectivity of the tissue at depth z. The factor of 2 in the exponential accounts for the light passing through the tissue twice after being backscattered. It should be noted that the optical depth is a measure of the depth in terms of the number of mean free path lengths, i.e. $\mu_s z$. $T(z)$ is linked to the local refractive index and backscattering property of the tissue (Tuchin 2000; Wang 2000). However, for a homogenous turbid medium it can be considered to be constant. Therefore, μ_t can be obtained theoretically from the reflectance measurements at two different depths, z_1 and z_2:

$$\mu_t = \frac{1}{2(\Delta z)} \ln\left(\frac{R(z_1)}{R(z_2)}\right) \tag{2}$$

where $\Delta z = |z_1 - z_2|$. As noise is inevitable in the measurement, a final result should thus be obtained by the use of a least-square fitting technique in order to improve the accuracy of the determined value of μ_t.

The OCT system used in this study employs a broadband light source, delivering an output power of 1 mW at the central wavelength of 820 nm with a bandwidth of 25 nm. The light source yields 12 μm axial resolution in free space that determines the imaging axial resolution of the system. A cross-sectional image is achieved by the combination of axial reflectance while the sample is scanned laterally. Polarization controllers are used to provide the maximum obtainable resolution for the given spectral width of the source. The beam spot size was measured at 16 μm, limited by the numerical aperture of the lens used to deliver the light onto the sample and the optical frequency of the incident light, as in conventional microscopy. The system has a measured signal-to-noise ratio of 97 dB at a scanning speed of 2 mm/s.

Materials

Liquid phantoms were first constructed to demonstrate the feasibility of the OCT system to quantify the absorption changes in tissue. The liquid phantoms consist of intralipid solution (Intralipid 10%, Pharmacia) mixed with different concentrations of naphthol green B (Sigma, N-7257), an effective absorber for the NIR light. A 0.75% intralipid solution was prepared to make the phantoms, with the concentration of naphthol green B ranging from 0 to 0.2%.

Human brain derived astrocytoma cells (7 and 20×10^6 per construct) were cultured in three dimensions using a 1.5% agarose gel. All cell-seeded constructs had a thickness of approximately 500 μm to 1 mm and were maintained in physiological saline during the monitoring procedure. In addition, perisoteal tissue from the calvaria of newborn (3-day old) and adult Wistar rats (>250 g) were harvested and cultured for up to 3 h in physiological saline prior to monitoring.

Measurements

Attenuation coefficient by OCT

The samples were mounted on a translation stage at the sample arm and were placed perpendicular to the probing beam. Repeat scans for one spatial point of each liquid phantom were performed, and reflected powers were averaged to minimize noise.

Firstly, cross-sectional signals were taken within the sample and the reflectivity from 20 lateral scans was averaged to minimize noise and treated as the control. After this measurement, for the sample with oxidized CytOx, 1% sodium dithionite in PBS solution was then applied to reduce CytOx in the same sample for 10 min. Another measurement was carried out for the sample with reduced enzyme. The difference in attenuation was calculated by subtracting the attenuation coefficient of the sample with oxidized enzyme from that of the reduced sample, i.e.:

$$\Delta\mu_t = \mu_t(\text{oxidized}) - \mu_t(\text{reduced}) \quad (3)$$

Histochemistry of CytOx in rat calvaria

Histochemical localization of CytOx was conducted as described by Kiernan (1990). Calvaria from 3-day-old rats were dissected and immersed in OCT compound (Tissue-Tek), a chemical for tissue frozen section, before immediately snap freezing in a dry ice/IMS/hexane (<160 °C) freezing bath, and then stored under liquid nitrogen. Cryostat sections were collected on slides and stored if necessary in an ultra-low-temperature freezer. Tissue sections were then stained for CytOx according to Kiernan (1990).

Biochemical determination of CytOx concentrations in cells and tissues

A biochemical assay (Brown et al. 1991) for cytochrome *a* was employed. Cytochrome *a* is an integral component protein of the cytochrome oxidase complex with one cytochrome *a* per cytochrome oxidase.

Between 0.3 and 0.5 g wet weight of tissue and cells per mL of ice-cold buffer (100 mM potassium phosphate, 2 mM EDTA, pH 7.1) was added. The suspension was homogenized and then stored on ice. Then 1 mL of homogenate was added to 1 mL of 20% w/w Triton X-100 and 1.5 mL of buffer, agitated and 3 mL of suspension was filtered through a 200 μm sieve. Detergent was present to reduce the light scattering of the samples. The difference at two wavelengths, 605 nm and 625 nm, was measured by a Cecil 3000 spectrophotometer. Cytochrome *a* was reduced by adding 30 μL of a mixture containing 0.1 M sodium cyanide, 0.1 M sodium ascorbate, and 5 mg *N*,*N*,*N*',*N*'-tetramethyl-*p*-phenylenediamine dihydrochloride (TMPD) per mL (pH 7.1). The difference in absorbance at 605/625 nm (before and immediately after addition of the reducing mixture) was used as a measure of the concentration of cytochrome *a* in the homogenates. The cytochrome *a* concentration was calculated using a (reduced minus oxidized) extinction coefficient at 605–625 nm of 20 mM^{-1} cm^{-1}.

Results

OCT imaging of periosteum overlying calvaria

Optical coherence tomograms of the backscattered power measured within a two-dimensional region of adult and newborn rat calvaria at 820 nm are shown in Fig. 2. The periosteum, cartilage/bone, endosteum and other features

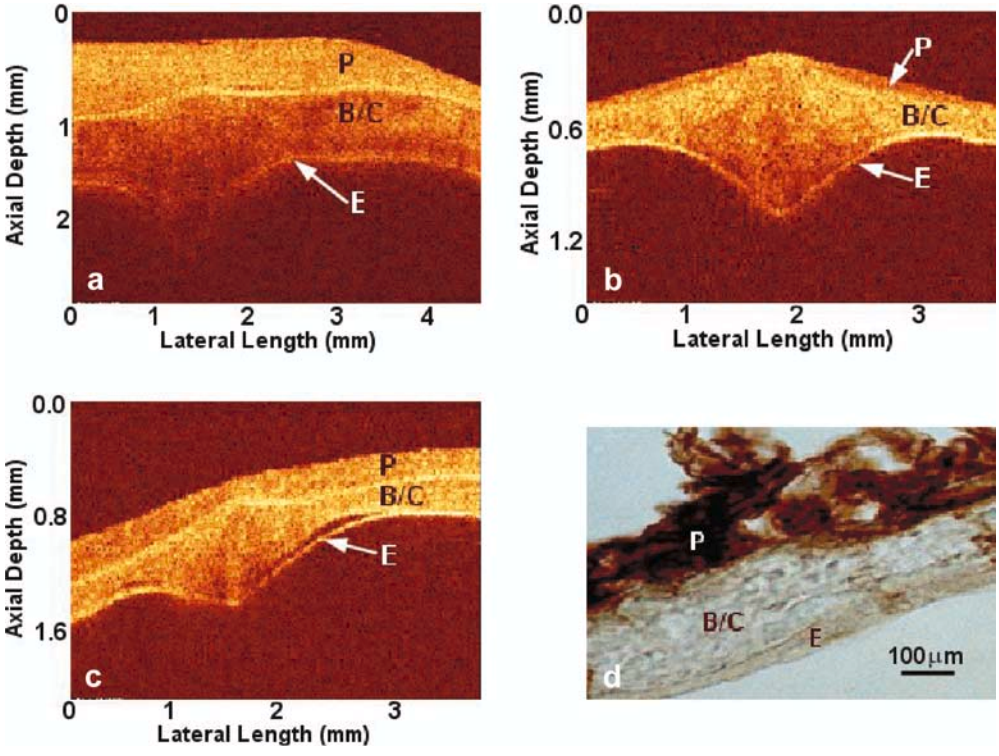

Fig. 2 OCT images captured from rat calvaria for (**a**) adult, (**b**) young and (**c**) new-born rat, where *P* represents the periosteum, and *B*/*C* the interface between bone and cartilage. Part (**d**) shows the result from the calvaria stained by histochemistry of cytochrome oxidase, where *P* is the periosteum, *B* the bone and *E* the endosteum

of the calvaria from both adult and newborn rats are sharply differentiated. The thickness of the periosteal layer increases with the rat age, and in the newborn rat the perisoteal depth was measured to be approximately 30 μm by the OCT system. Some brighter regions of the image result from variations in the density or orientation. Such results demonstrate that OCT is capable of high-resolution tomographic imaging of the skull or calvaria, which previously could only be obtained by conventional excisional biopsy. However, the cellular structure within the bone matrix of the specimens cannot be differentiated because both axial and lateral resolutions of the system exceed the widths of the cell layers in the tissue samples.

The OCT images of newborn rat calvaria correlated well with the histologic section (Fig. 2d), where three layers of periosteum, cartilage/bone and endosteum were apparent, as found from OCT images. Periosteal tissue was stained brown in the histochemical experiment, which indicated that periosteum is the tissue of cytochrome oxidase activity. It should be pointed out that the periosteal layer became loose and artificially thicker after the frozen section and stain process owing to its fragile nature. In addition, the histochemical picture was obtained only from a small section without a calvaria joint. It was difficult to obtain a large intact frozen section from the delicate newborn rat calvaria.

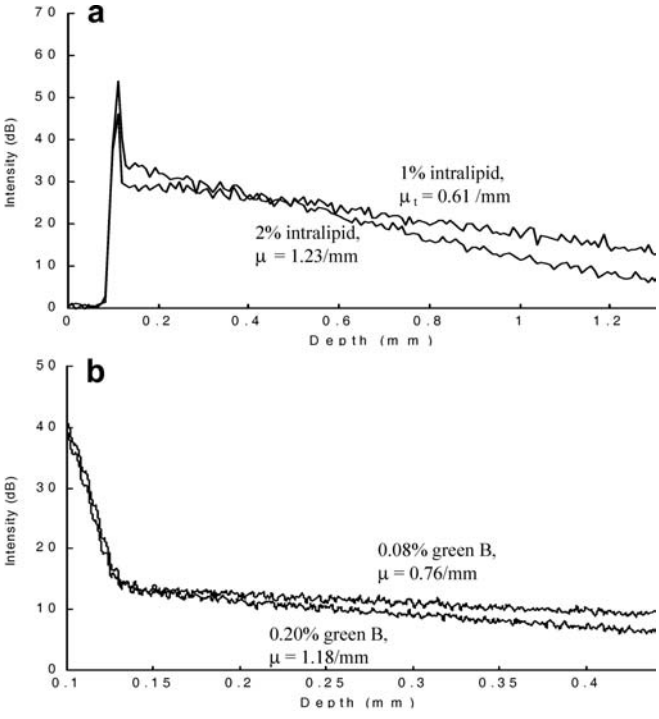

Fig. 3 Reflected signals from a liquid phantom at 820 nm by OCT measurement: (**a**) intralipid (scatter); (**b**) naphthol green B with 1% intralipid (absorber with scatter)

Attenuation measurements by OCT

Liquid phantoms

Naphthol green is an effective absorber for short NIR light (700–850 nm), is highly water soluble and introduces minimal scattering in the solution (Iizuka et al. 1999). Intralipid is often used as a scattering agent in tissue models. Thus in the first set of experiments the different concentrations of the dye solution mixed with intralipid were prepared and used as phantoms to simulate absorption changes in the tissue with the CytOx redox shift. Figure 3 shows reflectance versus depth profiles measured with OCT at 820 nm from (a) 1% and 2% intralipid solution only and (b) samples consisting of several different concentrations from 0.0025% to 0.2% of naphthol green B with 0.75% intralipid in water. It can be clearly seen from Fig. 3 that the backscattered signals recorded from all liquid phantoms appear straight on the semi-logarithmic plot and the reflected signals fell off exponentially with depth. The decay rates increased with the increase of scatter concentration (a) and absorber concentration (b) of the samples. According to the single scattering model, the slopes of the reflectance signals versus depth from the sample represent the total attenuation at that wavelength. The slopes were determined by fitting the backscattered power curves, plotted on a logarithmic scale as a function of the sample depth. The attenuation of the sample containing 2% intralipid ($\mu_t \approx 1.23$/mm) is higher than that of the sample with 1% intralipid ($\mu_t \approx 0.61$/mm) because of more scatter. The measured μ_t values are within the range

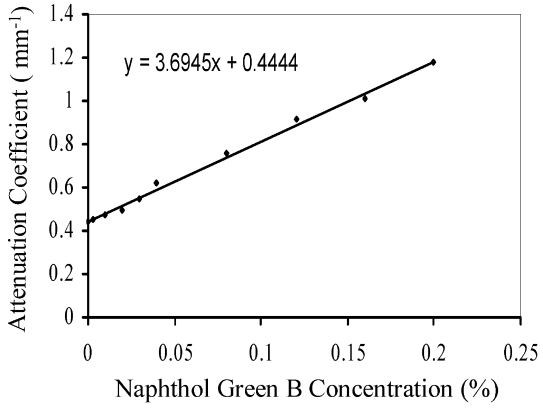

Fig. 4 Total attenuation coefficients of naphthol green B with 0.75% intralipid measured by optical coherence quantitation at 820 nm

of those obtained by van Staveren et al. (1991). The attenuation of the sample containing 0.20% naphthol green B ($\mu_t \approx 1.18$/mm) is higher than that of the sample with 0.08% naphthol green B ($\mu_t \approx 0.76$/mm) because of more absorption.

The total attenuation coefficients of different concentrations of naphthol green B solution mixed with 0.75% intralipid were calculated from the slopes of the curves, based on a single scattering model using a least-square curve-fitting method. Figure 4 shows the relationship between the total attenuation coefficient of sample solutions containing absorbers of various con-

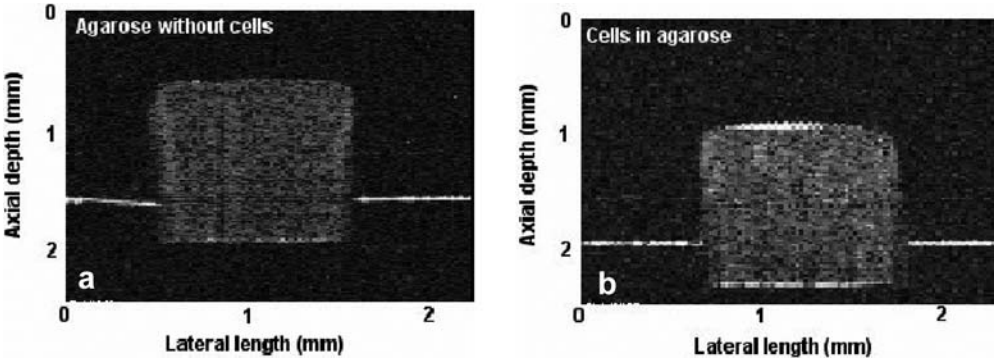

Fig. 5 OCT images of agarose (**a**) without and (**b**) with astrocytoma cells. The cells are seen as the bright spots in (**b**)

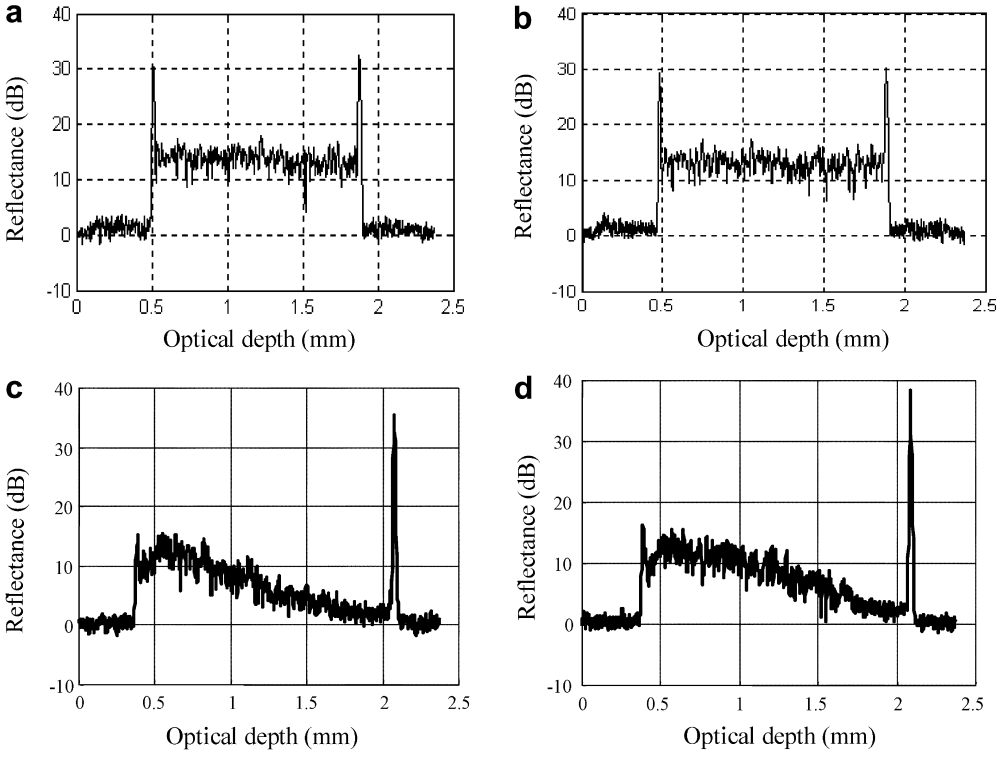

Fig. 6 Reflected signals measured by OCT from agarose without (*top*) and with astrocytoma cells (*bottom*), before (*left*) and after (*right*) the application of reducing agent

centrations and a naphthol green B concentration for dye content from 0 to 0.2%. The attenuation coefficients (μ_t) demonstrate a linear increase with the concentration of the dye. The coefficient appears to be an accurate measure of absorber concentration, even with a very low content down to a green B concentration of 0.0025%. By subtracting a scattering coefficient of 0.75% intralipid, the absorptivity of the dye was estimated to be 0.33 ± 0.05 mm^{-1} mM^{-1}, which is in good agreement with the value of 0.40 ± 0.02 mm^{-1} mM^{-1} measured by conventional transmission spectrophotometry.

Changes in attenuation in cultured cells with redox shift of CytOx

Astrocytoma cells were fixed in agarose plugs to simulate relatively homogeneous soft tissue without haemoglobin. OCT images of agarose without and with cells are shown in Fig. 5. The cells are seen as the bright spots in Fig. 5b. No attenuation within pure agarose (control) and no change before and after application of reducing agent were observed from the reflectivity versus depth profiles (Fig. 6a, b). The reflectance versus depth profiles of cell samples (Fig. 6c) showed that there was attenuation in cell-seeded agarose constructs. When the cells were reduced by sodium dithionite, the attenuation coefficient decreased (Fig. 6d). The first and second peaks in the profiles correspond to reflections at the air/sample and sample/glass slide interfaces, respectively. Attenuation coefficients of the oxidized form of CytOx within astrocytoma cell-seeded constructs were 0.41 ± 0.10 mm^{-1} ($n = 9$) for 7×10^6 cells and 0.54 ± 0.10 mm^{-1} ($n = 7$) for 20×10^6 cells, respectively. It should be pointed out that the attenuation coefficient does not scale with the number of cells but reflects the concentration, since the cells are within a

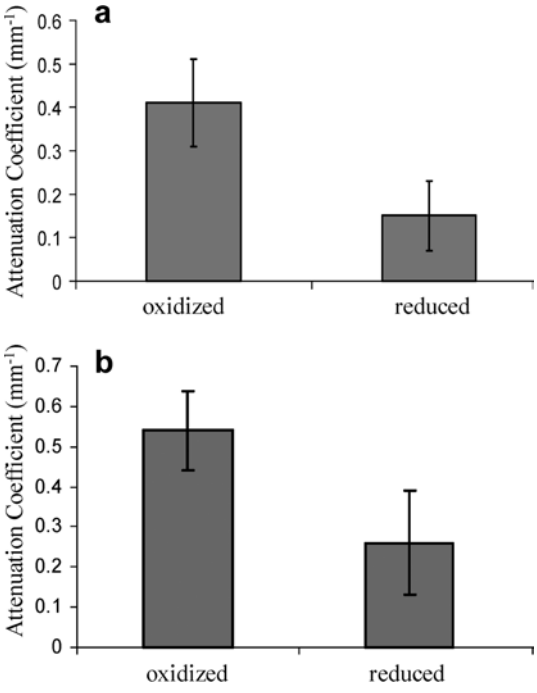

Fig. 7 Total attenuation coefficients measured at different redox states of CytOx in astrocytoma cells: (**a**) 7 million cells in an agarose plug, $n=7$; (**b**) 20 million cells in agarose, $n=7$

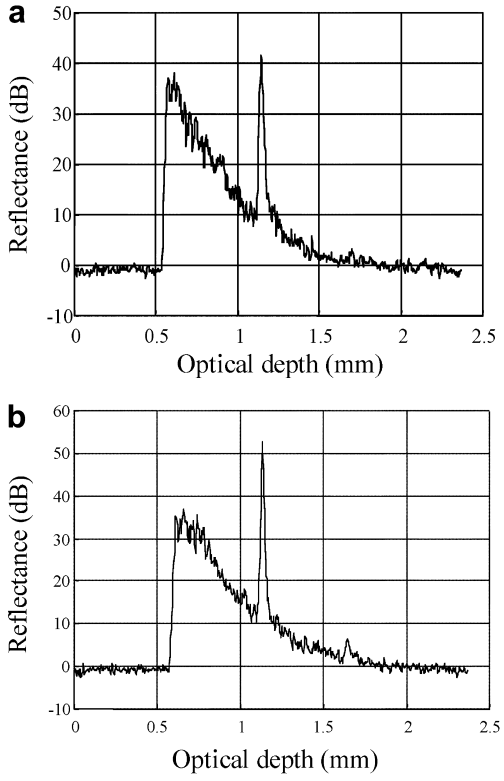

Fig. 8 Reflectance versus depth profile of periosteum with redox change of CytOx at 820 nm

fixed volume. In contrast, values obtained for the same sample with the reduced form of CytOx were 0.15 ± 0.08 mm^{-1} ($n=9$) and 0.26 ± 0.13 mm^{-1} ($n=7$), respectively. The difference between oxidized and reduced attenuation values is significant at both cell concentrations ($P<0.01$). The difference in attenuation of the astrocytoma cells before and after reduction of CytOx is calculated to be 0.26 ± 0.10 mm^{-1} ($n=9$) and 0.28 ± 0.13 mm^{-1} ($n=7$) according to Eq. (3), respectively (Fig. 7).

Changes in attenuation in tissues with redox shift of CytOx

The average of the reflected signal versus depth profiles from 20 spatial points through a periosteal tissue explant are plotted in Fig. 8a. The first and second peaks in the profile correspond to reflections at the air/tissue and tissue/glass slide interfaces, respectively. The distance between these two peaks corresponds to the measured displacement (z) of the reference mirror in air. The effective sample thickness is given by $d=z/n_s$, where n_s is the mean refractive index of the sample ($n_s=1.37$ as measured for the tissues used in this study). The averaged thickness of the samples ($n=7$) was determined to be $\sim 396 \pm 101$ μm; note that this thickness does not represent the real thickness of the periosteum in natural calvaria. The other distinct peaks in the measured profile were produced by each discontinuity in the refractive index in the sample. As predicted by the single-backscatter model in the ideal case of tenuous and relatively transparent tissues, the slopes of the reflectance-depth profile in the tissue represent the total attenuations of the periosteums with the oxidized form of CytOx.

To demonstrate the capability of the OCT system to extract information on changes in optical property, experiments were conducted by chemically reducing CytOx in tissues with sodium dithionite. The total attenuation was measured as a function of the reduction time. As an example, the reflectance versus depth (average of 10 scans) at the same spatial positions after CytOx was reduced for 10 min as shown in Fig. 8b. The result shows that the attenuation coefficient in the periosteum specimens is markedly decreased as CytOx is reduced. The mean attenuation coefficients of oxidized periostea were 2.48 ± 0.52 mm^{-1} ($n=7$), whilst reduction of the explant tissue resulted in a reduced mean value of 2.05 ± 0.60 mm^{-1} ($n=7$). The difference in the attenuation coefficient of the oxidized and reduced tissues (0.43 ± 0.24 mm^{-1}; $n = 7$) is significant ($P<0.05$).

Biochemical assays

The concentrations of CytOx in astrocytoma cells and adult rat periosteum determined by a biochemical assay were 7.2 ± 1.3 μM ($n=4$) and 7.6 ± 2.2 μM ($n=4$), respectively. Cytochrome *a* appeared to be fully oxidized in cultured cells before addition of the reducing mixture, as

addition of 2 μL rotenone and antimycin resulted in no significant change. The concentration of CytOx with addition of rotenone and antimycin was 7.5 ± 1.2 μM ($n = 4$) and 7.6 ± 1.7 μM ($n = 4$), respectively. A small increase for the periosteum of rat with addition of rotenone (9.2 ± 1.7 μM; $n = 4$) and antimycin (8.8 ± 1.2 μM; $n = 4$) was observed. Cytochome *a* in the periosteal samples was not fully oxidized, which may reflect differences in the in vivo state versus cells grown in culture. The difference in absorption coefficients of oxidized/reduced CytOx at 820 nm in astrocytoma cells and the periostea were estimated to be $8.3 \pm 1.5 \times 10^{-3}$ mm^{-1} ($n = 4$) and $8.7 \pm 2.5 \times 10^{-3}$ mm^{-1} ($n = 4$) by the equation $\mu_a = 2.303 \epsilon c$, where ϵ is the extinction coefficient of the oxidized/reduced form of cytochrome oxidase, approximately 0.5 mm^{-1} mM^{-1} at 820 nm according to Matcher et al. (1995).

Discussion

A beam of light progressively attenuates as it penetrates into a turbid biological tissue by absorption and scattering of the tissue. Haemoglobin and oxidized CytOx are the main absorbers that can indicate the tissue oxygenation state in most soft tissues in the NIR wavelength region. Scattering loss comes from, on a microscopic scale, a variety of cellular structures including cell organelles, the cell nucleus, organized cell structures and interstitial layers, etc. The homogenous liquid phantoms, containing a range of concentrations of absorbers and scatterers, demonstrate well the capabilities of OCT for measuring quantitatively the total attenuation and absorption coefficients.

The reflectance curves measured in this study from periostea overlying calvaria tissues were not as consistent as those assessed from liquid phantoms. The prominent irregularities in the curves presumably resulted from local variations due to the heterogeneous property of most soft tissues. Incomplete averaging of coherent speckle and random noise probably also account for the irregularity in the profiles of periosteal tissue, but changes in the exponential slopes of reflectance signals versus depth after reduction of CytOx was clearly evident.

A comparison of the oxidized/reduced absorption coefficient of CytOx from the biochemical assays with the attenuation coefficient in cells and periosteum using OCT has demonstrated a difference in magnitude in the measurements. The shift in the coefficient of astrocytoma cells and periosteum at 0.26 mm^{-1} and 0.43 mm^{-1} as measured using the OCT would correspond to a concentration of about 230 μM and 370 μM of cytochrome oxidase, respectively, while the values measured by biochemical analysis are less than 10 μM. Although the qualitative shifts correlated with oxidation states of the biological samples are observed using both methodologies, the amplified values would suggest that the measurement made by OCT definitely does not solely come from the CytOx activity.

One explanation for this discrepancy in values may be due to the specificity of the OCT measurements for cytochrome *a* when compared with biochemical assay. There is evidence that the spectral changes seen in the 780–900 nm NIR region of mitochondria are over 80% due to cytochrome oxidase *CuA* with the remainder being due to cytochrome *c*, cytochrome *b*, and the various oxygenated intermediates of cytochrome oxidase (Thörnström et al. 1988). Therefore, the OCT measurements could include a 20% amplification from the CytOx assay measurements.

This would not account fully for the discrepancy and it is likely that variation in the cell scattering properties may potentially result from treatment with the reducing agent. Results from Liu et al. (1996) show that addition of a solute to tissue may affect the cell volume or shape as well as the refractive indices of the extra- and intracellular fluids, and thus ultimately influence the overall tissue scattering properties. The action of sodium dithionite may influence the cell hydration and swelling, which could change the size or shape of the scattering centres, thereby affecting the variation of the light scattering.

Our results demonstrate that qualitative shifts in the oxidative state of cells can be monitored in real time using the OCT system. However, using these parameters to calculate the concentration of cytochrome oxidase present in tissues may result in exaggerated values as a result of the influence of scattering and specificity for one enzyme within the oxidative cascade. Recently, the use of an OCT system with a dual-wavelength has been explored to quantify the water absorption within the turbid medium (Schmitt et al. 1998), where two wavelengths were deliberately chosen to span the water absorption band and reduce the scattering effect. Such a method may be useful in future studies to monitor the redox state of tissues, which will enable the scattering changes to be discriminated. It is clear that further studies are needed to separate the absorption changes from the scattering changes in cells and tissues. Nevertheless, OCT, with further development, does offer a potential combined technique for visualization of the microstructures of periosteal explants and cell-seeded constructs with micron-scale resolution alongside an assessment of the cellular activity levels, which may have applications in cell biological research and tissue engineering.

Acknowledgements This research was made possible with financial support from the EPSRC for the project GR/R52978 and GR/N13715, and from the European Union for the BITES project.

References

Brown GC, Crompton M, Wray S (1991) Cytochrome oxidase content of rat brain during development. Biochim Biophys Acta 1057:273–275

Delpy DT, Cope M (1997) Quantification in tissue near-infrared spectroscopy. Philos Trans R Soc London Ser B 352:649–659

Iizuka MN, Sherar MD, Vitkin AI (1999) Optical phantom materials for near infrared laser photocoagulation studies. Lasers Surgery Med 25:159–169

Jöbsis FF (1977) Noninvasive, infrared monitoring of cerebral and myocardial oxygen sufficiency and circulatory parameters. Science 198:1264–1267

Kiernan JA (1990) Histological & histochemical methods: theory & practice. Pergamon Press, Oxford, pp 258–287

Liu H, Beauvoit B, Kimura M, Chance B (1996) Dependence of tissue optical properties on solute-induced changes in refractive index and osmolarity. J Biomed Opt 1:200–211

Matcher SJ, Elwell CE, Cooper CE, Cope M, Delpy DT (1995) Performance comparison of several published tissue near-infrared spectroscopy algorithms. Anal Biochem 227:54–68

Morgner U, Drexler W, Kärtner FX, Li XD (2000) Spectroscopic optical coherence tomography. Opt Lett 25:111–113

Sathyam US, Colston BW, Da Silva LB, Everett MJ (1999) Evaluation of optical coherence quantitation of analytes in turbid media by use of two wavelengths. Appl Opt 38:2097–2104

Schmitt JM, Knüttel A, Bonner RF (1993a) Measurement of optical properties of biological tissues by low-coherence reflectometry. Appl Opt 32:6032–6042

Schmitt JM, Knüttel A, Gandjbakhche A, Bonner RF (1993b) Optical characterization of dense tissues using low-coherence interferometry. Proc SPIE 1889:197–211

Schmitt JM, Xiang SH, Yung KM (1998) Differential absorption imaging with optical coherence tomography. J Opt Soc Am A 15:2288–2296

Staveren HJ van, Moes CJM, Marle J van, Prahl SA, Gement JC van (1991) Light scattering in Intralipid-10% in the wavelength range of 400–1100 nm. Appl Opt 30:4507–4514

Tearney GJ, Brezinski ME, Bouma BE, Boppart SA, Fujimoto JG (1997) In vivo endoscopic optical biopsy with optical coherence tomography. Science 276:2037–2039

Thörnström PE, Brzezinski P, Fredriksson PO, Malmstrom BG (1988) Biochemistry 27:5441–5447

Tuchin V (2000) Tissue optics: light scattering methods and instruments for medical diagnosis. (Tutorial texts in optical engineering, vol 38) SPIE, Bellingham, Wash., USA

Tuchin VV, Xu X, Wang RK, (2002) Dynamic optical coherence tomography in studies of optical clearing, sedimentation and aggregation of immersed blood, Appl Opt 41:258–271

Tzagoloff A (1982) Mitochondria. Plenum Press, New York

Wang RK (1999) Resolution improved optical coherence-gated tomography for imaging through biological tissues. J Mod Opt 46:1905–1912

Wang RK (2000) Modelling optical properties of soft tissue by fractal distribution of scatters. J Mod Opt 47:103–120

Wang RK, Elder JB (2002a) High resolution tomographic imaging of soft biological tissues. Int J Laser Phys 12:17–22

Wang RK, Elder JB (2002b) Propylene glycol as a contrasting medium for optical coherence tomography to image gastrointestinal tissues. Lasers Surgery Med 30:201–208

Wang RK, Xu X, Tuchin VV, Elder JB (2001) Concurrent enhancement of imaging depth and contrast for optical coherence tomography by hyperosmotic agents, J Opt Soc Am B 18:948–953